Budapesti University of Technology and Economics
Faculty of Mechanical Engineering
Department of Hydrodynamic Systems

Modelling Arterial Blood Flow and its Application in Medical Diagnostics

Booklet of the PhD Dissertation

Written by: Viktor Szabó

Applied Mathematics (MSc)

Supervisor: Dr. Gábor Halász

Professor Emeritus

07 September 2017, Budapest

1 DETECTING HYPOVOLEMIA USING ARTERIAL BLOOD PRESSURE

1.1 Introduction

Hypovolemia occurs when the volume of blood circulating in the human body decreases. Normovolemia refers to the state when the volume is normal. The most common errors in the management of patients who died in hospital were related to inadequate fluid resuscitation [1]–[3]. It remains a difficult task to predict the hemodynamic profile using conventional parameters [4]. To recognize the adequacy of volume status of critically ill patients, a complete evaluation of the hemodynamic profile is recommended [5]–[7].

In this study an attempt is made to predict the volume of blood using the arterial blood pressure graph. The advantage of such a method is that, unlike most hemodynamic parameters, blood pressure can be accessed non-invasively, and therefore could lead to the early detection of the hypovolemia.

1.2 Methods

Blood pressure was measured before (HYPO) and after (NORMO) fluid rescuscitation in 18 postoperative hypovolemic patients.

From each measurement, a cardiac cycle was chosen randomly. Using the Fast Fourier Transformation (FFT), the mean average pressure (MAP) as well as the phase (PHI1-PHI8) and the amplitude (A1-A8) of the first 8 harmonics were calculated.

Using paired sample t-test, it was shown that the values of MAP, A1 and PHI1 were different in HYPO and NORMO groups ($p<0,01$) (Table 1.1). In case of A1 the difference was very significant ($p<0,001$).

				95% confidence interval	
Parameter	**Group**	**Mean**	**Standard deviation**	**Lower bound**	**Upper bound**
MAP (mmHg)	*HYPO*	78.98	12.44	72.79	85.17
	NORMO	88.11	9.91	83.19	93.04
A1 (mmHg)	*HYPO*	18.09	5.44	15.38	20.79
	NORMO	24.29	5.45	21.58	27.00
PHI1 (rad)	*HYPO*	−1.52	0.14	−1.59	−1.45
	NORMO	−1.61	0.14	−1.68	−1.54

Table 1.1 Descriptive statistics for variables MAP, A1 and PHI1. Note that the 95% confidence interval for A1 is disjoint in hypovolemic and normovolemic cases.

Using logistic regression, 28 new patients were categorized into hypovolemic and normovolemic groups based on the values of MAP, A1 and PHI1 using different methods. Among the patients, 14 were hypovolemic and 14 were normovolemic.

Best results were achieved when categorization was performed using only the values of A1 (Table 1.2). Using this method, decision was made in case of 10 out of 14 hypovolemic patients (71%), 8 out of which (that is, in 80% of the decisions) were correct, and 2 (20% of the decisions) were incorrect. In case of normovolemic patients, decision was made in case of 5 patients (35%); 2 correct (40%), and 3 incorrect (60%).

Group (original):	HYPO (n=14)			NORMO (n=14)		
Group (predicted):	HYPO	NORMO	No decision	HYPO	NORMO	No decision
Method 1	4	1	9	1	0	13
Method 2	6	1	7	4	0	10
Method 3	8	2	4	3	2	9

Table 1.2 Results of categorization in different scenarios for hypovolemic and normovolemic patients

1.3 Summary

It was found that the amplitude of the first Fourier harmonic calculated from the blood pressure is significantly different between hypovolemic and normovolemic patients. The difference of this new hemodynamic parameter was more significant than that of the mean average pressure. The advantage of this parameter that and it can be calculated from the blood pressure graph using the Fast Fourier Transform. The corresponding thesis (Thesis 1) can be found in chapter 5.

2 MODELLING THE EFFECT OF BODY MOTION IN ARTERIAL NETWORKS

2.1 Introduction

Most of the time our bodies are in motion. During walking, travelling, or sports we are exposed to body acceleration. Since the 80's, numerous studies have been conducted to analyse the effect of motion on blood flow [8], [9]. Most of them, however – with a few exceptions [10], [11] – considered only one artery. In most cases the effect of motion is taken into account by modifying the gravitational term in the momentum equation using the cosine function. We are not aware of any publications studying the effect of motion on arterial blood flow with viscoelastic wall behaviour.

2.2 Methods

A previously published 1D blood flow model developed by the Department of Hydrodynamic Systems has been modified to study mobile arterial networks [12], [13]. To take the effect of motion into account, the momentum equation was solved numerically in a coordinate system relative to the vessel segments and was modified by the inertial force term denoted by f_x:

$$\frac{\partial w}{\partial t} + w\frac{\partial w}{\partial x} + \frac{1}{\rho}\frac{\partial p}{\partial x} + g\frac{dh}{dx} + f_x + \frac{32\nu}{D^2}w = 0 \quad (1)$$

where w denotes the velocity of blood particles relative to the vessel segment (m/s), D the diameter (m), p the transmural pressure (Pa), h the elevation (m), ν the kinematic viscosity (m^2/s), g the gravitational acceleration (m/s^2), ρ the density of the blood (kg/m^3).

The original model was validated against measured pressure data acquired from a distributed physical model [14]. The modified model was validated in an accelerating and a rotating vessel segment where blood pressure could be calculated analytically. In both cases, good agreement was found between simulation results and the analytical solution.

Because of the lack of literature data, several physiological effects of motion could not be taken into account. The limitations of the model are discussed in detail in chapter 2.2.4.

2.2.1 Cycling

First, the effect of cycling motion on arterial blood flow was analysed using the updated model [15]. The motion of the legs has been modelled by the four-link mechanism. Simulations were performed at different levels of angular velocity (ω). The increase of velocity resulted an increased blood flow in the ankles and in the aorta but did not change significantly the flow in the shoulders (Table 2.1). The motion had significant effect on the blood pressure (Fig. 2.1) but only a minor effect on the average values. Blood pressure and blood flow graphs showed qualitative agreement.

ω (Hz)	aorta	shoulder	ankle
0.0	5.095	0.326	0.074
0.5	5.101	0.326	0.078
1.0	5.137	0.326	0.081
1.5	5.142	0.326	0.085
2.0	5.191	0.326	0.087

Table 2.1 Average blood flow (l/min) in different levels of angular velocity

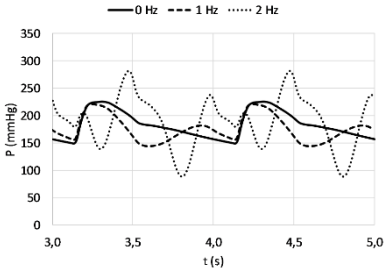

Figure 2.1 Blood pressure in the lower leg

2.2.2 Arm circumdiction

Next, the effect of arm circumdiction has been analysed [16]. The arms performed a rotating motion at different levels of angular velocity (ω) between 0 and 2 Hz. The angle between the arms in the upper and lower positions (α) changed between 50° and 150° (Fig. 2.3). Blood flow at the aorta slightly increased with the increase of the velocity and the decrease of the angle, which can be explained by the increase of the centrifugal force as a result of the rotating motion (Table 2.2). The motion had significant effect on the blood pressure (Fig. 2.2). Neither the angular velocity nor the angle had any effect on the blood flow in the abdominal aorta; it was 1.96 l/min in all cases.

ω (Hz)	heart	50°	100°	150°
	0.5	5.03	5.04	5.04
	1.0	5.13	5.11	5.07
	1.5	5.20	5.16	5.10
	2.0	5.41	5.32	5.17

ω (Hz)	wrist	50°	100°	150°
	0.5	0.029	0.029	0.029
	1.0	0.041	0.038	0.033
	1.5	0.055	0.048	0.036
	2.0	0.076	0.063	0.043

Table 2.2 Average blood flow (l/min) in the heart and in the wrist

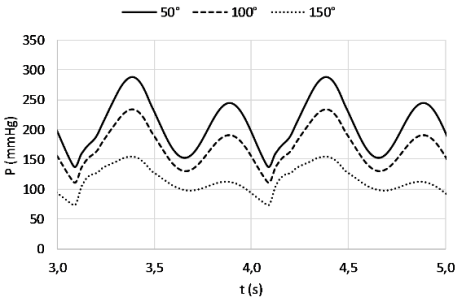

Figure 2.2 Blood pressure calculated in the wrist during maximum rotation (2 Hz)

2.2.3 Running

In the case of running, gait analysis was performed using the VICON Nexus gait analysis system (Vicon Motion Systems, Oxford, UK). 12 markers were attached to the body of a volunteer (Fig. 2.4). Using a treadmill, measurements were performed between 0 and 12 km/h with 1 km/h increments. In each case, the 3D positions of each marker were recorded with a frequency of 100 Hz. For each measurement, the average heart rate was also recorded.

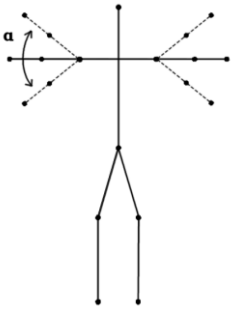

Figure 2.3. Simplifed model of arm circumdiction. The immobile case is denoted by the horizontal line (α=0°). In the model only the motion of the arms was considered.

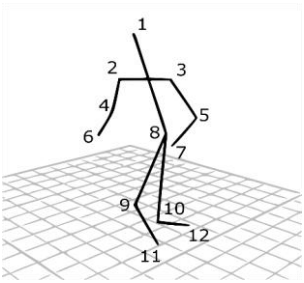

Figure 2.4 Gait analysis using the VICON Nexus software. The biomarkers were attached to the head (1), the shoulders (2-3), the elbows (4-5), the wrists (6-7), the hip (8), the knees (9-10), and the ankles (11-12).

The position of each vessel was calculated from the position of the biomarkers. At the heart, periodic flow rate was used as a proximal boundary condition, which was modified according to the heart rate based on previous measurements [17].

The average blood pressure in the lower leg was 10.09 m/s^2 at maximum speed (12 km/h), which is more than the gravitational acceleration.

The oscillation of blood pressure in the wrist, and especially in the foot increased significantly (Fig. 2.5). The effect of motion on the average blood pressure was less

significant: e.g. in the left foot average pressure increased by only 5%, and the increase was even less in other arteries. However, in the left foot the oscillation of blood pressure increased by more than 200% compared to the immobile case (Fig. 2.6). The average blood flow and blood pressure showed qualitative agreement.

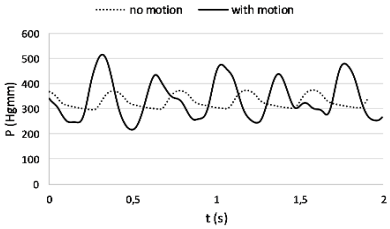

Figure 2.5 Blood pressure in the left foot calculated at maximum speed including (solid line) and omitting (dotted line) the effect of motion.

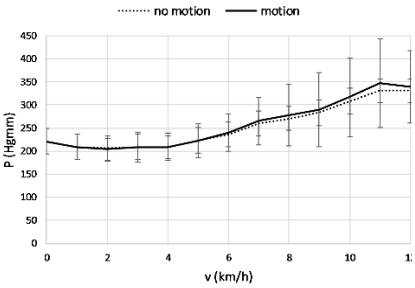

Figure 2.6 Average blood pressure in the left foot calculated at different levels of speed including (solid line) and omitting (dotted line) the effect of motion. The standard deviation is represented by the error bars.

2.2.4 Limitations

In this study only the mechanical effects of motion was analysed. Among the physiological effects only the change of the heart rates was considered. While it is known that the exercise has a significant effect e.g. on the vessel diameter [18] and the total peripheral resistance [19], and the presence of local vascular control mechanism also has an effect on the blood flow [18], these could not be included in the model because currently there are not enough measurement data in the literature describing these effects that could be used for a reliable simulation.

2.3 Summary

A model has been presented to analyse blood flow in mobile arterial networks. The hemodynamic equations were solved in a coordinate system relative to the vessel segments, and the effect of motion was taken into account by including an inertial force term into the momentum equation. In simple cases good agreement was found between simulation results and the analytical solution. Using the method presented above, the applicability of other 1-D models can also be extended from immobile to mobile arterial networks. The corresponding theses (Thesis 2 and Thesis 3) can be found in chapter 5.

3 EFFECT OF CARDIAC MOTION ON CORONARY BLOOD FLOW

3.1 Introduction

Analysing coronary blood flow is a well researched area. This can be explained by the fact that cardiovascular diseases (CVDs) are the number 1 cause of death globally [20]. CVDs are commonly caused by atherosclerosis that can hamper or even stop blood flow. It has been shown that vessel deformation (torsion, rotation) plays an important role in developing atherosclerosis [21]–[24]. Thus modelling coronary blood flow is an important task. In the past several studies modelling the effect of cardiac motion have been published. Yet we have found no such 1D model that would consider blood flow in a coronary arterial network with viscoelastic wall properties.

3.2 Methods

The blood flow model presented in the previous chapter has been modified and used to study the effect of cardiac motion in the main coronary arteries of patients diagnosed with coronary arterial disease (CAD). At the inlet, aortic pressure was prescribed as a periodic boundary condition. At the terminal sites – unlike in the previous cases – the so called 3-element Windkessel model developed by Westerhof et al [25], [26] was applied instead of the linear resistance model.

Vessel geometry was acquired from computer tomography (CT) images using the MEDIS medical image processing software. CT images were recorded for 3 patients. For each patient 10 measurements were performed in different phases of the cardiac cycle (systole and diastole) (Fig. 3.1). For each measurement, the centerline of the three main coronary arteries (RCA, LAD, LCX) and the average diameter has been calculated in 10-20 points.

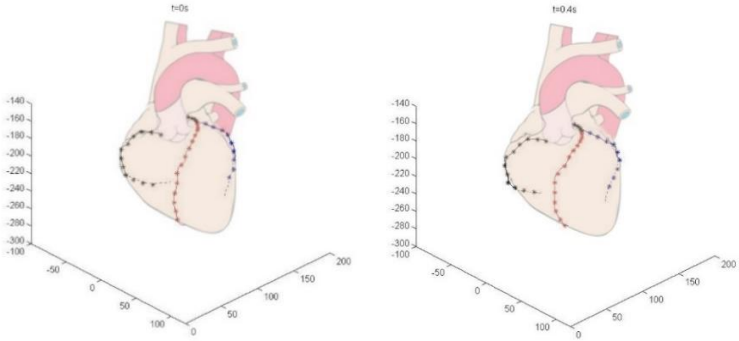

Figure 3.1 Coronary arterial network of a patient during systole (left) and diastole (right) using the artwork of Patrick J. Lynch[1]

[1] Patrick J. Lynch, medical illustrator derivative work: Fred the Oyster (talk) adaption and further labeling: Mikael Häggström (Coronary.pdf) CC BY-SA 3.0, via Wikimedia Commons

Using the 3D positions measured at different phases, cardiac motion has been reconstructed. For every numerical point, the gravitational ($g\frac{dh}{dx}$) and the inertial (f_x) force term has been calculated.

Since the heart rate was not available, an initial heart rate of 60 was chosen. The translation of the vessel was only a few mm (Fig. 3.1) therefore a higher heart rate of 150 was set to amplify the effect of cardiac motion. The aortic pressure at the inlet was modified accordingly.

Average blood pressure and flow has been calculated for each patient at both heart rates, including as well as omitting the effect of cardiac motion.

3.3 Results

The effect of gravitational force was significantly higher than that of the inertial force. Including the cardiac motion had little effect either on flow velocity (<0.01 m/s) (Table 3.1) or on blood pressure (<2 mmHg) (Table 3.2).

		Patient 1		Patient 2		Patient 3	
v (m/s)		**A)**	**B)**	**A)**	**B)**	**A)**	**B)**
Mobile	**LCX**	0.21	0.33	0.10	0.18	0.25	0.45
	LAD	0.17	0.38	0.09	0.16	0.14	0.14
	RCA	0.14	0.21	0.15	0.18	0.14	0.22

Table 3.1 Average flow velocity calculated at heart rate of 60 (A) and 150 (B) including the effect of motion. Omitting the effect of motion had little (<0.01 m/s) effect on the results.

		Patient 1		Patient 2		Patient 3	
P (mmHg)		**A)**	**B)**	**A)**	**B)**	**A)**	**B)**
Mobile	**LCX**	104.6	229.4	100.9	226.4	100.1	223.4
	LAD	103.4	228.9	104.1	226.0	101.1	226.0
	RCA	103.9	228.3	102.6	225.9	103.1	228.6
Immobile	**LCX**	104.5	228.0	100.9	226.4	100.2	225.5
	LAD	103.4	227.9	104.1	227.1	101.1	226.0
	RCA	103.8	229.2	102.5	227.2	103.4	229.1

Table 3.2 Average blood pressure calculated at heart rate of 60 (A) and 150 (B)

3.4 Summary

The effect of cardiac motion on coronary blood flow was analysed using the model presented in the previous chapter. The only difference was that at the terminal sites the

so called 3-element Windkessel model was applied as a boundary condition. Including the effect of motion had little effect either on flow velocity or blood pressure which indicates that cardiac motion has little effect on coronary blood flow. This is in concordance with previous results from 3D models [27], [28], but at a significantly lower computational cost. The corresponding thesis (Thesis 3) can be found in chapter 5.

4 MODELLING BLOOD PRESSURE IN STENOSED CORONARY ARTERIES

4.1 Introduction

As it has been mentioned in the previous chapter, cardiovascular diseases (CVDs) are caused by atherosclerosis, that is the narrowing and/or blockage of the coronary blood vessels. In the recent years, fractional flow reserve (FFR) has emerged as a reliable index for determining the significance of a coronary stenosis [29]. It is the ratio of the distal to the proximal pressure before the stenosis:

$$\frac{\overline{\Delta p_{st}}}{\overline{p_{prox}}} = \frac{\overline{p_{prox}} - \overline{p_{dist}}}{\overline{p_{prox}}} = 1 - \frac{\overline{p_{dist}}}{\overline{p_{prox}}} = 1 - FFR \tag{2}$$

In clinical trials, the value of FFR below 0.8 is generally recommended as a threshold for a revascularisation [30]. While most studies aim to calculate the value of FFR non-invasively [31]–[33], recent studies suggest that not only the value of FFR but also the blood pressure waveform contains important information about the nature of the flow in a stenosed coronary artery [34]–[36].

4.2 Methods

In the previous chapter it has been shown that cardiac motion has no significant effect on the coronary blood flow. Therefore, the effect of motion has not been included in the model. At the inlet, the proximal pressure was used as a periodic boundary condition. The stenosis as well as the arterioles were taken into account using the linear resistance model (Fig. 4.1).

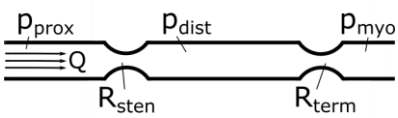

Figure 4.1 Simplified model of the stenosis. The linear resistance model was applied both at the stenosis (R_{sten}) and the terminal sites (R_{term}).

The original model has been successfully used when the linear resistance at the outlet was constant [12]. Coronary arteries, however, are squeezed by the heart during contraction. Therefore, either time-varying peripheral resistance or time-varying pressure should be prescribed at the outlet. Calculating time-varying resistance for the 5 patients did not prove to be useful, therefore we applied time-varying pressure at the outlet.

The myocardial pressure (p_{myo}) at the outlet was calculated from the pressure in the left ventricle (p_{LV}). Ghista has used the following an analytic model to approximate ventricular radial stress $\sigma(r)$ as a function of left ventricular pressure [37]:

$$\sigma(r) = p_{LV} \frac{r_i^3}{r_e^3 - r_i^3}\left(1 - \frac{r_e^3}{r^3}\right), \tag{3}$$

where r_i and r_e denotes the inner and outer radius of the left ventricle (m), respectively. Using this approximation – assuming normal dimensions for the left ventricle – the average stress was $0{,}44 \cdot p_{LV}$. In our model, the average myocardial pressure was approximated by the average stress, that is 44% of the left ventricular pressure p_{LV}.

To calculate the value of p_{LV}, the so-called time-varying elastance model was used, which was first introduced by Suga [38], and was first applied to the coronary circulation by Krams [39]. It has been successfully used in earlier studies for the modelling of the left ventricle [40], [41]. In this model the ventricular elastance E_{LV} (Pa/m^3) is defined as the ratio of p_{LV} to the left ventricular volume V_{LV} (m^3), corrected for a "dead volume" V_0 (m^3), the volume in the ventricle at zero pressure:

$$E_{LV}(t) = \frac{p_{LV}(t)}{V_{LV}(t) - V_0} \tag{4}$$

The left ventricular pressure is calculated in each cardiac phase differently [42]. The different phases can be seen in Fig. 4.2.

Phase I - Isovolumetric contraction: The beginning phase of the contraction lasts between the closing of the mitral valve (a) and the opening of the aortic valve (b). During this phase the left ventricle is completely full and its volume is maximal, therefore p_{LV} can be calculated using the following formula:

$$p_{LV}(t) = E_{LV}(t) \cdot (V_{max} - V_0) \tag{5}$$

Several models can be used to approximate elastance during this phase. For the studied patients best results were achieved using the sinusoid approximation [42]:

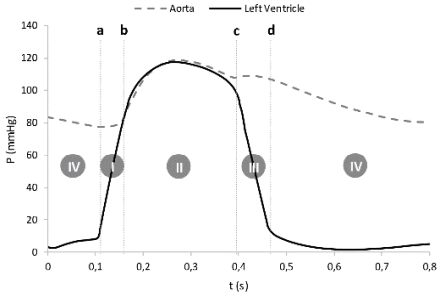

Figure 4.2 Blood pressure in the aorta and the left ventricle during different phases of the cardiac cycle (adapted from Fonyó [43])

$$E_{LV}(t) = E_{max} \cdot \sin\left(\frac{t\pi}{2T_{rise}}\right) \qquad (6)$$

where T_{rise} is ca. 83% of the duration of systole and E_{max} is the ratio between the blood pressure measured during the closing of the aortic valve (c) and the minimal volume difference:

$$E_{max} = \frac{p_c}{V_{min} - V_0} \qquad (7)$$

Phase II – Ventricular ejection: This phase lasts between at the opening (b) and the closing (c) of the aortic valve during systole. During this phase the pressure in the ventricle is similar to the aortic pressure, and therefore can be used for estimating p_{LV}.

Phase III - Isovolumetric relaxation: This phase lasts between the closing of the aortic valve (c) and the opening of the mitral valve (d) during early diastole. During this phase the volume of left ventricle is minimal, and therefore p_{LV} (4) is calculated using the following formula:

$$p_{LV}(t) = E_{LV}(t) \cdot (V_{min} - V_0). \qquad (8)$$

Elastance is calculated using the sinusoid approximation [42]:

$$E_{LV}(t) = E_{max} \cdot \left(1 - \sin\left(\frac{(t - T_{rise})\pi}{2T_{fall}}\right)\right) \qquad (9)$$

where T_{fall} is ca. 17% of the duration of systole and E_{max} is calculated similar to Phase I.

Phase IV – Ventricular filling: This phase lasts between the opening (d) and the closing (a) of the mitral valve during diastole. During this phase the left ventricular pressure is approximately 0, and therefore the elastance is 0.

The minimal volume of the left ventricle V_{min} was set to 40 ml, and the maximal volume V_{max} to 120 ml. These values did not have significant effect on the results. Using the pressure at the opening and closing of the aortic valve during systole – that is at (b) and (c) in Fig. 4.2, respectively, the value of V_0 can be calculated as:

$$V_0 = \frac{p_b V_{min} - E_b p_c V_{max}}{p_b - E_b p_c} \qquad (10)$$

where E_b is the normalized elastance that is calculated at (b) in Fig. 4.2:

$$E_b = \frac{E_{LV}(t_b)}{E_{max}} = \sin\left(\frac{t_b \pi}{2T_{rise}}\right) \tag{11}$$

4.2.1 Measurement data

The geometry of 5 stenosed coronary vessels were acquired from two appropriate projections of the invasive coronary angiography (Fig 4.3). Consecutive patients were studied with a wide range of suspected or known coronary artery diseases, which were referred to the Hemodynamic Laboratory of University of Debrecen, Department of Cardiology and Cardiac Surgery. All patients underwent a diagnostic coronary angiography at the centre according to the local protocol. Coronary angiographies were performed through the radial or femoral access according to the feasibility of the radial approach or the patient suitability and operator preference. All patients gave written informed consent to the invasive procedure in accordance with the protocol approved by the local ethics committee.

Average diameter and length was calculated after the 3D reconstruction by a dedicated software. In addition, proximal and distal blood pressure were measured, from which the value of FFR was determined.

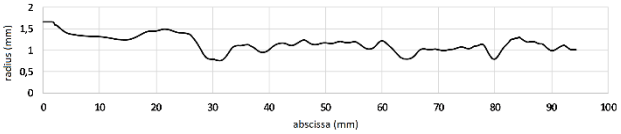

Figure 4.3 Radius of vessel segment from patient BME4

For each patient, blood flow was calculated using vessel geometry and the propagation speed of the contrast dye (Table 4.1).

Using measurement data, the value of stenosis resistance (R_{sten}) and terminal resistance (R_{term}) was calculated in the following way: first, the average value of the total pressure drop was calculated as the difference between the average proximal pressure and the average myocardial pressure:

$$\Delta p_{total} = \overline{p_{prox}} - \overline{p_{myo}} = \overline{p_{prox}} - 0{,}44 \cdot \overline{p_{LV}} \tag{12}$$

The pressure drop is caused by the resistance at the stenosis and the terminal site as well as the friction loss along the vessel (Δp_{fric}), which – assuming laminar flow – can be calculated by the following:

$$\Delta p_{fric} = \frac{32 \cdot \nu \cdot L \cdot \rho \cdot v}{D^2}, \tag{13}$$

where ν denotes the kinematic viscosity ($3 \cdot 10^{-6}$ m^2/s), L the vessel length (m), ρ the density of blood (1050 kg/m^3), v the blood velocity (m/s), and D the instantaneous value of the vessel diameter (m), depending on the pressure.

After decreasing the total pressure loss by the friction loss, the sum of the stenosis and terminal resistance (Ns/m^5) can be calculated as the ratio of the remaining pressure loss to the average blood flow Q:

$$R_{sten} + R_{term} = \frac{\Delta p_{total} - \Delta p_{fric}}{Q} \tag{14}$$

The sum of the resistances can be determined after calculating the value of the right hand side of the formula. Next, the sum was divided into two parts so that the distal blood pressure and the average blood flow calculated from the simulation results would approximate the measured data. The values of resistances and the measured as well as the calculated FFR values can be seen in Table 4.1.

For the simulation, patient-specific parameters were used based on the vessel geometry and measurement data. Elastic properties of the vessel also has an effect on the distal blood pressure graph but up to 50% changes in the value ofs the elastic modulus had little effect on the results.

4.3 Results

Calculated FFR values and blood flow showed very good agreement with measurement data (Table 4.1). The root mean squared error (RMSE) between measured and calculated distal blood pressure was less than 9 mmHg for each patient, which accounted for 3-13% of the average distal pressure.

Patient	L (mm)	Q (ml/s)		FFR (-)		R_{sten} (Ns/m^5)	R_{term} (Ns/m^5)	RMSE (mmHg)
		Measured	Calculated	Measured	Calculated			
BME1	85	2,88	2,89	0,53	0,53	1,73E+09	1,49E+09	5,40 (8%)
BME2	75	3,49	3,48	0,87	0,85	5,25E+08	2,49E+09	2,91 (3%)
BME3	51	3,21	3,23	0,81	0,84	1,05E+08	1,79E+09	8,81 (13%)
BME4	94	2,73	2,79	0,93	0,92	3,15E+08	4,52E+09	6,94 (5%)
BME10	88	4,66	4,65	0,73	0,73	3,78E+08	9,98E+08	4,45 (8%)

Table 4.1 Measured and calculated values of FFR and blood flow. The ratio of the RMSE to the average distal blood pressure is denoted by parentheses.

Measured and calculated distal blood pressure graphs can be seen in Fig. 4.4. Qualitative agreement was found for each patient. The agreement was very good in case of patients BME1, BME2 and BME4.

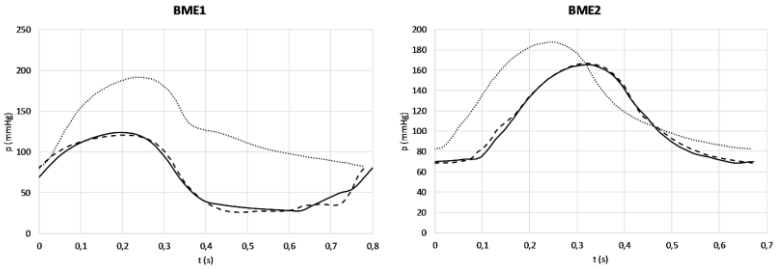

Figure 4.4 Proximal (dotted), measured distal (dashed), and simulated distal (solid) blood pressure graphs of patients BME1 and BME2

4.4 Summary

The model presented above can be used to approximate distal blood pressure in stenosed coronary arteries. For the simulation, patient-specific parameters were used based on the vessel geometry and measurement data. Measured and calculated distal blood pressure graphs show good agreement. One of the main advantages of this model is that, using patient-specific parameters, the distal blood pressure can be calculated for different values of average blood flow at the inlet. The average simulation time is less than 2 minutes on a personal computer which makes it possible to perform parameter studies and analyse the effect of blood flow on the distal blood pressure. This can provide useful information for medical research [34]–[36]. The corresponding thesis (Thesis 4) can be found in chapter 5.

5 THESIS POINTS

Thesis #1

The amplitude of the first Fourier-harmonic of the arterial blood pressure graph is lower for hypovolemic patients than to normovolemic ones (p<0,001), therefore it is a useful parameter to detect hypovolemia.

Corresponding publications [43], [44]:

- Viktor Szabo; Gabor Halasz, CSc; Tibor Gondos, MD, CSc: Detecting hypovolemia in postoperative patients using a discrete Fourier transform. Computers in Biology and Medicine (IF: 1.475) (DOI:10.1016/j.compbiomed.2015.01.018)
- Szabó Viktor; Gondos Tibor; Halász Gábor: Matematikai statisztikai módszerek alkalmazása vérnyomásgrafikonok elemzésére. OGÉT 2014-XXII. Nemzetközi Gépészeti Találkozó. 2014. pp. 347-350.

Thesis #2

The mechanical effect of motion in arterial networks can be modelled by solving the momentum equation and the momentum equation in a coordinate system relative to the vessel segments. The effect of motion can be taken into account by including an inertial force term into the momentum equation. The modified form of the momentum equation can be written as:

$$\frac{\partial w}{\partial t} + w\frac{\partial v}{\partial x} + \frac{1}{\rho}\frac{\partial p}{\partial x} + g\frac{dh}{dx} + f_x + \frac{32\nu}{D^2}w = 0 \qquad (15)$$

where w denotes the velocity of blood particles relative to the vessel segment (m/s), D the diameter (m), p the transmural pressure (Pa), h the elevation (m), ν the kinematic viscosity (m^2/s), g the gravitational acceleration (m/s^2), ρ the density of the blood (kg/m^3).

The values of f_x can be calculated from the motion of the vessel segment.

Corresponding publication [45]:

- V. Szabó and G. Halász: 1-D blood flow modelling in a running human body, Computer Methods in Biomechanics and Biomedical Engineering, pp. 1–8, Apr. 2017.

Thesis #3

Using the model presented in Thesis #2, the following statements can be made:

- In the case of cycling motion or arm circumduction, at the speed of 2 revolutions per second, the oscillation of the blood pressure in the rotating limbs increases by a factor of two compared to the static case.
- In the case of running at the speed of 12 km/h, the average blood pressure in the lower limb arteries increases with less than 5%, but their oscillation increases by a factor of three.

- At a heart rate of 150, the mechanical effect of the cardiac motion has little (<1%) influence on the average blood flow rate and blood pressure, therefore the coronary arterial network can be assumed to be static during simulations.

Corresponding publications: [15], [16], [46]:

- V. Szabó, G. Halász: Effect of Arm Circumduction on Arterial Blood Flow. First European Biomedical Engineering Conference for Young Investigators (ENCY2015) (ISBN: 978-981-287-572-3)
- Viktor Szabó, Gábor Halász: Effect Of Cycling Motion On Human Arterial Blood Flow. Conference on Modelling Fluid Flow (CMFF'15), (ISBN:978-963-313-190-9)
- Szabó Viktor; Halász Gábor: Szívmozgás hatása szívkoszorúerekben keringő vér áramlására. OGÉT 2016-XXIV. Nemzetközi Gépészeti Találkozó. 2016. pp. 398-401.

Thesis #4

In stenosed coronary arteries, patient-specific values of linear resistances modelling terminal sites (R_{term}) and the stenosis (R_{sten}) can be calculated using the vessel geometry, the value of the average blood flow (Q), and the proximal (p_{prox}) and distal (p_{dist}) blood pressure:

1. The average myocardial pressure (i.e. the average ventricular radial stress) can be approximated by 44% of the left ventricular pressure $p_{LV}(t)$.
2. The average value of the total pressure drop can be calculated as the difference between the average proximal pressure and the average myocardial pressure:

$$\Delta p_{total} = \overline{p_{prox}} - \overline{p_{myo}} = \overline{p_{prox}} - 0{,}44 \cdot \overline{p_{LV}} \tag{16}$$

3. The time-dependent value of the left ventricular pressure can be defined using the so called time-varying elastance model as the product of the ventricular elastance E_{LV} and the left ventricular volume V_{LV} corrected for a "dead volume" V_0, the volume in the ventricle at zero pressure:

$$p_{LV}(t) = E_{LV}(t) \cdot (V_{LV}(t) - V_0) \tag{17}$$

4. To elastance can be calculated using the sinusoid approximation published by Vandenberghe [42] using the proximal blood pressure graph.
5. The sum of the stenosis and terminal resistance can be calculated as the ratio of the total pressure loss decreased by the friction loss to the average blood flow:

$$R_{sten} + R_{term} = \frac{\Delta p_{total} - \Delta p_{fric}}{Q}, \tag{18}$$

6. Using simple manual optimization, the resistance values can be acquired by dividing the sum into two parts so that the distal blood pressure and the average blood flow calculated from the simulation results would approximate the measured data.

Using the model presented above, blood pressure graphs can be simulated where measurement is not possible considering ethical limitations.

Corresponding publication [47]:

- V. Szabó, C. Jenei, and G. Halász, "Modelling Blood Pressure in Stenosed Coronary Arteries," Period. Polytech. Mech. Eng., 2017.

6 IRODALOMJEGYZÉK

[1] S. A. Deane, P. L. Gaudry, P. Woods, D. Cass, M. J. Hollands, R. J. Cook, and C. Read, "The management of injuries--a review of deaths in hospital.," *Aust. N. Z. J. Surg.*, vol. 58, no. 6, pp. 463–469, 1988.

[2] A. Sauaia, F. A. Moore, E. E. Moore, K. S. Moser, R. Brennan, R. A. Read, and P. T. Pons, "Epidemiology of trauma deaths: a reassessment.," *J. Trauma*, vol. 38, no. 2, pp. 185–93, Feb. 1995.

[3] D. S. Kauvar, R. Lefering, and C. E. Wade, "Impact of hemorrhage on trauma outcome: an overview of epidemiology, clinical presentations, and therapeutic considerations.," *J. Trauma*, vol. 60, no. 6 Suppl, pp. S3–S11, 2006.

[4] A. L. Holder, G. Clermont, and M. R. Pinsky, "Early Identification of Occult Bleeding Through Hypovolemia Detection," in *Annual Update in Intensive Care and Emergency Medicine*, vol. 2014, J.-L. Vincent, Ed. Springer International Publishing, 2014, pp. 555–567.

[5] T. Gondos, "Volumetriás hemodinamikai monitorozás," *Aneszteziológia és Intenzív Terápia*, vol. 30, no. S1, pp. 2–11, 2000.

[6] G. Marx and T. W. L. Scheeren, "Advanced hemodynamic monitoring in the critically ill patient: Nice to have or need to treat?," *Journal of Clinical Monitoring and Computing*, vol. 30, no. 5, pp. 1–2, Oct-2016.

[7] R. C. Pacagnella, J. P. Souza, J. Durocher, P. Perel, J. Blum, B. Winikoff, and A. M. Gülmezoglu, "A Systematic Review of the Relationship between Blood Loss and Clinical Signs," *PLoS ONE*, vol. 8, no. 3. 2013.

[8] V. K. Sud and G. S. Sekhon, "Blood flow subject to a single cycle of body acceleration," *Bull. Math. Biol.*, vol. 46, no. 5–6, pp. 937–949, Sep. 1984.

[9] A. Zaman, N. Ali, and M. Sajid, "Numerical simulation of pulsatile flow of blood in a porous-saturated overlapping stenosed artery," *Mathematics and Computers in Simulation*, vol. 134, pp. 1–16, 2017.

[10] V. K. Sud and G. S. Sekhon, "Analysis of blood flow through a model of the human arterial system under periodic body acceleration.," *J. Biomech.*, vol. 19, no. 11, pp. 929–41, Jan. 1986.

[11] D. S. Sankar and A. K. Nagar, "Nonlinear Fluid Models for Biofluid Flow in Constricted Blood Vessels under Body Accelerations: A Comparative Study," *J. Appl. Math.*, vol. 2012, 2012.

[12] G. Bárdossy and G. Halász, "A 'backward' calculation method for the estimation of central aortic pressure wave in a 1D arterial model network," *Comput. Fluids*, vol. 73, pp. 134–144, Mar. 2013.

[13] G. Bárdossy and G. Halász, "Modeling blood flow in the arterial system," *Period. Polytech. Mech. Eng.*, vol. 55, no. 1, p. 49, May 2011.

[14] F. Molnár, S. Till, and G. Halász, "Arterial blood flow and blood pressure

measurements at a physical model of human arterial system," in *3rd European Medical and Biological Engineering Conference - EMBEC'05*, 2005, pp. 1–7.

[15] V. Szabó and G. Halász, "Effect of cycling motion on human arterial blood flow," in *Proceedings of Conference on Modelling Fluid Flow (CMFF'15)*, J. Vad, Ed. Budapest: CFD.HU Kft, 2015, p. Paper 104. 4 p.

[16] V. Szabó and G. Halász, "Effect of Arm Circumduction on Arterial Blood Flow," in *First European Biomedical Engineering Conference for Young Investigators*, vol. 50, Á. Jobbágy, Ed. Singapore: Springer Singapore, 2015, pp. 87–90.

[17] V. Gemignani, E. Bianchini, F. Faita, M. Giannoni, E. Pasanisi, E. Picano, and T. Bombardini, "Assessment of cardiologic systole and diastole duration in exercise stress tests with a transcutaneous accelerometer sensor," in *2008 Computers in Cardiology*, 2008, pp. 153–156.

[18] D. N. Ku, "Blood flow in arteries," *Annu. Rev. Fluid Mech.*, vol. 29, no. 1, pp. 399–434, Jan. 1997.

[19] R. Hambrecht, A. Wolf, S. Gielen, A. Linke, J. Hofer, S. Erbs, N. Schoene, and G. Schuler, "Effect of exercise on coronary endothelial function in patients with coronary artery disease.," *N. Engl. J. Med.*, vol. 342, no. 7, pp. 454–60, Feb. 2000.

[20] WHO, "WHO Cardiovascular diseases (CVDs)," *Cardiovascular diseases (CVDs)*, 2016. [Online]. Available: http://www.who.int/mediacentre/factsheets/fs317/en/. [Accessed: 03-Jan-2017].

[21] J. Friedman, T. Hastie, and R. Tibshirani, *The Elements of Statistical Learning: Data Mining, Inference, and Prediction.*, vol. 1. Springer, 2009.

[22] Z. Ding and M. H. Friedman, "Dynamics of Human Coronary Arterial Motion and Its Potential Role in Coronary Atherogenesis," *J. Biomech. Eng.*, vol. 122, no. 5, p. 488, Oct. 2000.

[23] Z. Ding, H. Zhu, and M. H. Friedman, "Coronary Artery Dynamics In Vivo," *Ann. Biomed. Eng.*, vol. 30, no. 4, pp. 419–429, Apr. 2002.

[24] Y. Qiu and J. M. Tarbell, "Numerical Simulation of Pulsatile Flow in a Compliant Curved Tube Model of a Coronary Artery," *J. Biomech. Eng.*, vol. 122, no. 1, p. 77, Feb. 2000.

[25] N. Westerhof, F. Bosman, C. J. De Vries, and A. Noordergraaf, "Analog studies of the human systemic arterial tree," *J. Biomech.*, vol. 2, no. 2, pp. 121–143, May 1969.

[26] M. Zamir, *The Physics of Coronary Blood Flow*. Springer US, 2006.

[27] A. Theodorakakos, M. Gavaises, A. Andriotis, A. Zifan, P. Liatsis, I. Pantos, E. P. Efstathopoulos, and D. Katritsis, "Simulation of cardiac motion on non-Newtonian, pulsating flow development in the human left anterior descending coronary artery.," *Phys. Med. Biol.*, vol. 53, no. 18, pp. 4875–92, Sep. 2008.

[28] D. Zeng, Z. Ding, M. H. Friedman, and C. R. Ethier, “Effects of cardiac motion on right coronary artery hemodynamics.,” *Ann. Biomed. Eng.*, vol. 31, no. 4, pp. 420–9, Apr. 2003.

[29] N. H. J. Pijls, W. F. Fearon, P. A. L. Tonino, U. Siebert, F. Ikeno, B. Bornschein, M. van’t Veer, V. Klauss, G. Manoharan, T. Engstrøm, K. G. Oldroyd, P. N. Ver Lee, P. A. MacCarthy, and B. De Bruyne, “Fractional flow reserve versus angiography for guiding percutaneous coronary intervention in patients with multivessel coronary artery disease: 2-year follow-up of the FAME (Fractional Flow Reserve Versus Angiography for Multivessel Evaluation) study.,” *J. Am. Coll. Cardiol.*, vol. 56, no. 3, pp. 177–84, Jul. 2010.

[30] B. De Bruyne, N. H. J. Pijls, J. Bartunek, K. Kulecki, J. W. Bech, H. De Winter, P. Van Crombrugge, G. R. Heyndrickx, and W. Wijns, “Fractional flow reserve in patients with prior myocardial infarction.,” *Circulation*, vol. 104, no. 2, pp. 157–162, 2001.

[31] E. Boileau, S. Pant, C. Roobottom, I. Sazonov, J. Deng, X. Xie, and P. Nithiarasu, “Estimating the accuracy of a reduced-order model for the calculation of fractional flow reserve (FFR),” *Int. j. numer. method. biomed. eng.*, Jun. 2017.

[32] S. Gaur, K. A. Øvrehus, D. Dey, J. Leipsic, H. E. Bøtker, J. M. Jensen, J. Narula, A. Ahmadi, S. Achenbach, B. S. Ko, E. H. Christiansen, A. K. Kaltoft, D. S. Berman, H. Bezerra, J. F. Lassen, and B. L. Nørgaard, “Coronary plaque quantification and fractional flow reserve by coronary computed tomography angiography identify ischaemia-causing lesions,” *Eur. Heart J.*, vol. 37, no. 15, pp. 1220–1227, 2016.

[33] K. Tanaka, H. G. Bezerra, S. Gaur, G. F. Attizzani, H. E. Bøtker, M. A. Costa, C. Rogers, and B. L. Nørgaard, “Comparison Between Non-invasive (Coronary Computed Tomography Angiography Derived) and Invasive-Fractional Flow Reserve in Patients with Serial Stenoses Within One Coronary Artery: A NXT Trial substudy,” *Ann. Biomed. Eng.*, vol. 44, no. 2, pp. 580–589, 2016.

[34] Z. Kőszegi, C. Jenei, J. Sánta, P. Sánta, and B. Tar, “Relation between fractional flow reserve and the intracoronary pressure waveform,” *Eur. 2015*, 2015.

[35] M. Vavuranakis, I. Stamatopoulos, T. G. Papaioannou, S. Nikolopoulos, K. Toutouzas, and C. Stefanadis, “Alterations of pressure waveforms along the coronary arteries and the effect of microcirculatory vasodilation,” *Int. J. Cardiol.*, vol. 117, no. 2, pp. 254–259, 2007.

[36] P. Lugosi, J. Santa, P. Santa, Z. Beres, B. Tar, P. Polgar, and Z. Koszegi, “Nonhyperemic intracoronary pressure waveform analysis predicts the fractional flow reserve,” *2010 Computers in Cardiology*. pp. 1079–1082, 2010.

[37] D. N. Ghista, L. Zhong, R.-S. Tan, and E. Y. K. Ng, “Left Ventricular Filling Performance Characteristics,” in *Cardiac perfusion and pumping engineering*, D. Ghista and E. Ng, Eds. Singapore: World Scientific Publishing Company Pte Limited, 2007, pp. 191–213.

[38] H. Suga, K. Sagawa, and A. A. Shoukas, “Load Independence of the Instantaneous

Pressure-Volume Ratio of the Canine Left Ventricle and Effects of Epinephrine and Heart Rate on the Ratio," *Circ. Res.*, vol. 32, no. 3, pp. 314–322, Mar. 1973.

[39] R. Krams, P. Sipkema, and N. Westerhof, "Varying elastance concept may explain coronary systolic flow impediment," *Am J Physiol Hear. Circ Physiol*, vol. 257, no. 5, pp. H1471-1479, Nov. 1989.

[40] P. Reymond, F. Merenda, F. Perren, D. Rüfenacht, and N. Stergiopulos, "Validation of a one-dimensional model of the systemic arterial tree.," *Am. J. Physiol. Heart Circ. Physiol.*, vol. 297, no. 1, pp. H208-22, Jul. 2009.

[41] J. P. Mynard and J. J. Smolich, "One-Dimensional Haemodynamic Modeling and Wave Dynamics in the Entire Adult Circulation," *Ann. Biomed. Eng.*, Apr. 2015.

[42] S. Vandenberghe, P. Segers, and P. R. Verdonck, "Mathematical Modeling of Ventricular-Assist Devices," in *Cardiac perfusion and pumping engineering*, D. N. Ghista and E. Y.-K. Ng, Eds. Singapore: World Scientific Publishing Company Pte Limited, 2007, pp. 419–475.

[43] V. Szabó, G. Halász, and T. Gondos, "Detecting hypovolemia in postoperative patients using a discrete Fourier transform," *Comput. Biol. Med.*, vol. 59, pp. 30–34, Apr. 2015.

[44] V. Szabó, T. Gondos, and G. Halász, "Matematikai statisztikai módszerek alkalmazása vérnyomásgrafikonok elemzésére," in *OGÉT 2014-XXII. Nemzetközi Gépészeti Találkozó*, 2014, pp. 347–350.

[45] V. Szabó and G. Halász, "1-D blood flow modelling in a running human body," *Comput. Methods Biomech. Biomed. Engin.*, vol. 9, pp. 1–8, Apr. 2017.

[46] V. Szabó and G. Halász, "Szívmozgás hatása szívkoszorúerekben keringő vér áramlására," in *OGÉT 2016-XXIV. Nemzetközi Gépészeti Találkozó*, 2016, pp. 398–401.

[47] V. Szabó, C. Jenei, and G. Halász, "Modelling Blood Pressure in Stenosed Coronary Arteries," *Period. Polytech. Mech. Eng.*, vol. 2, 2017.